A NOVEL ROTOR RESISTANCE IDENTIFICATION IN SLIP FREQUENCY CONTROLLED BEARINGLESS INDUCTION MOTORS

Daigo Akamatsu, Akira Chiba
Department of Electrical Engineering Faculty of Science and Technology,
Tokyo University of Science, 2641 Yamazaki, Noda, Chiba, Japan, 278-8510
Email: chiba@ee.noda.tus.ac.jp

Tadashi Fukao
Department of Electrical Engineering, Faculty of Technology,
Musashi Institute of Technology, 1-28-1, Tamazutsumi, Setagaya-ku, Tokyo, Japan 158-8557

ABSTRACT

Bearingless induction motors have combined characteristics of an induction motor and magnetic bearings. Induction motors tend to suffer influence of rotor resistance variation under field oriented control. Several rotor resistance identifications have been proposed in the literature. In this paper, a novel rotor resistance identification method based on variables in magnetic suspension loops is proposed. The rotor resistance is identified from suspension force command variations under static force generation in order to suspend a shaft weight. Thus, real time on-line identification is possible under the temperature variation.

INTRODUCTION

Magnetic bearings have been used in machine tools, turbo-molecular pumps, canned motor pumps, flywheels and compressors. The advantages of magnetic bearings are clear: maintenance is less troublesome, without grease and friction. However, conventional magnetic bearings have significant dimensions and require a number of wirings as well as many single phase inverters. To solve these problems, bearingless motors have been actively researched and developed in recent years.

Bearingless motors are an integration of a magnetic bearing with the function of a motor. Therefore, the advantages are small size and low-cost. Several types of motors have been proposed as bearingless motors, such as induction[1],[2],[3], surface mounted PM[4], inset PM[5], interior and buried PM[6], consequent-pole[7],[8], homopolar[9] and hybrid, synchronous reluctance[10] and switched reluctance[11] bearingless motors. Especially, induction motors are robust, low-cost and open loop operation provides nearly constant rotational speed. In addition, torque ripple and cogging torque are less. Thus, there is a strong need of induction bearingless motors in industries.

In the magnetic suspension of the bearingless motors, suspension forces are generated based on the feedback signals of displacement sensors detecting the movement of a rotor shaft. The suspension forces are generated taking an advantage of the strong flux distribution of a revolving magnetic field in the airgap between the stator and rotor. Thus, information of the instantaneous orientation and amplitude of the revolving magnetic field is required in a controller of the bearingless motor. Therefore, vector control methods are necessary for transient conditions. The vector control methods are divided roughly into two methods, i.e., flux detection and slip frequency control. In the latter case, flux detectors are unnecessary, however it is sensitive to parameter variations, especially a rotor resistance. If parameter settings are different from genuine values, performance is not very good. Especially, a rotor resistance is likely to depending on operating conditions. Thus, many researchers have proposed identification methods of a rotor resistance identification based on an observer, instantaneous reactive power, sinusoidal d-axis current and etc.

A novel rotor resistance identification method based on variables in magnetic suspension loops has been proposed by the authors[12]. The proposed method is based on suspension force commands, which are automatically generated by negative feedback loops. Successful operation of a test rotor resistance identification system has been demonstrated for a 4-pole bearingless motor. In this paper, the proposed method is implemented in a 2-pole bearingless induction motor. Theoretical expressions for a 2-pole test machine are derived. Successful operation is demonstrated. In addition, it is shown that the rotating shaft is successfully suspended with magnetic force, while the system temperature is increased. The effectiveness of the proposed system is shown.

SYSTEM CONFIGURATION

A. Principle of Suspension Force Generation

The basic winding configurations of an induction-type bearingless motor are shown in Figure 1. Two sets of three phase windings are wound in the same stator slots. One is the 2-pole windings for the production of motoring torque. The other is the 4-pole windings for controlling the rotor radial position in the airgap. These windings are referred as motor and suspension windings, respectively. The 2-pole flux Ψ_2 and 4-pole flux Ψ_4 are generated by the winding currents I_2 and I_4, respectively. The x and y are the stationary perpendicular axes.

Under no-load balanced condition, if positive suspension force along the y-axis is needed, the suspension winding current I_4 must be fed as shown in Figure 1. The flux density in the upper airgap is increased because both Ψ_2 and Ψ_4 fluxes are in the same direction. On the other hand, the flux density in the lower airgap is decreased because Ψ_2 and Ψ_4 are in opposite direction. A positive suspension force F is produced in the y-axis direction only. The reverse current can produce the opposite suspension force. Suspension force in the x-axis direction can be produced using electrically perpendicular 4-pole current distribution in the same principle.

Figure 2 shows a situation when actual Ψ_2 is advanced at an angle of θ_g by the incorrectly identified rotor resistance. There exists a phase difference between Ψ_2 and Ψ_4 fluxes. Consequently, suspension force is generated in the wrong direction of θ_f. Magnetic suspension may fail if force direction error θ_f has a serious discrepancy. To avoid this situation, the rotor resistance identification is necessary.

When $R_r^*=R_r$, the θ_g and θ_f are zero. When a rotor temperature rises, θ_g and θ_f are increased. This fact suggests that R_r^*/R_r can be identified when θ_f is measured while known static external force is applied. The θ_f is easy to measure on-line as suspension force commands are generated in the suspension controller. Static external force can be a shaft weight an in horizontal machine. In the experiment, a shaft weight was the external static force. A proposed rotor resistance identification system is constructed by using this principle.

B. Controller System Block Diagram

Figure 3 shows the block diagram of a field oriented control system of an airgap flux oriented vector controller system. Generally, vector control system flux is aligned with the rotor or stator flux linkage. In bearingless induction motors, the suspension force is produced by active unbalance of the airgap flux distribution between the rotor and stator. Therefore, electromagnetic force of magnetic suspension is originated from an interaction of the airgap fluxes. Thus, an airgap flux oriented vector control system is applied to bearingless induction motors[13],[14].

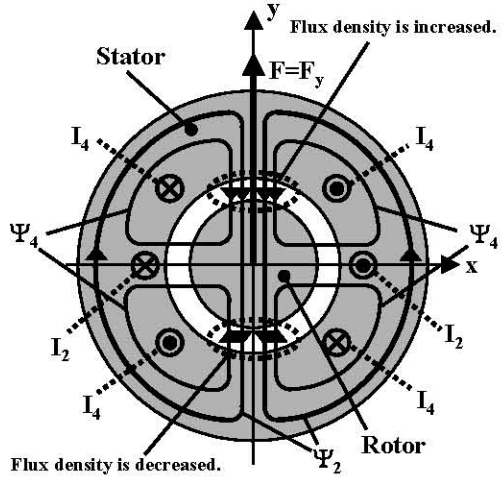

FIGURE 1: Principle of suspension force generation

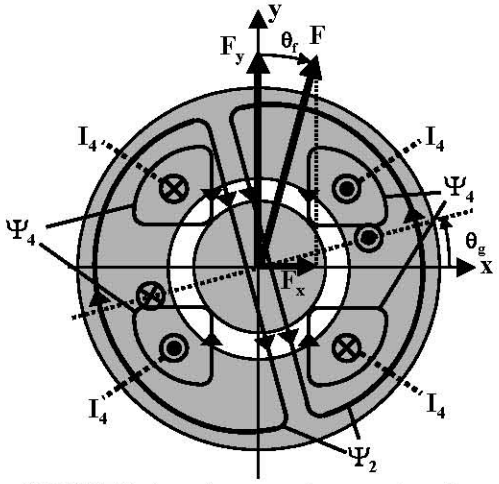

FIGURE 2: Interference of suspension force

The shaft speed ω_{rm} is detected and speed errors are calculated. The error is amplified in a Proportional-Integral(PI) controller. A torque component current command i_{qs}^* is generated. The superscript * indicates reference values. A flux current component i_{dm}^* is given as a constant. The d-axis current i_{ds}^* and the slip angular frequency ω_{se}^* are calculated from i_{qs}^* and i_{dm}^*. If a reference value R_r^* of the rotor resistance is exactly the same as actual value R_r, then the airgap flux linkage is kept in a constant amplitude. In addition, the speed of the airgap flux linkage is ω_0, where ω_0 is a sum of ω_{se}^* and the detected electrical rotor speed ω_{re}. Thus, components of the airgap flux linkage in x- and y-axes are following to the triangular functions $\Psi_c=\cos\phi_0$ and $\Psi_s=\sin\phi_0$, respectively. The signal $\cos\phi_0$ and $\sin\phi_0$ are hereafter referred as the controller flux references Ψ_c and Ψ_s, respectively. The triangular functions are used in the modulation block of the suspension controller. These signals are supposed to indicate the instantaneous flux components having a contribution in suspension

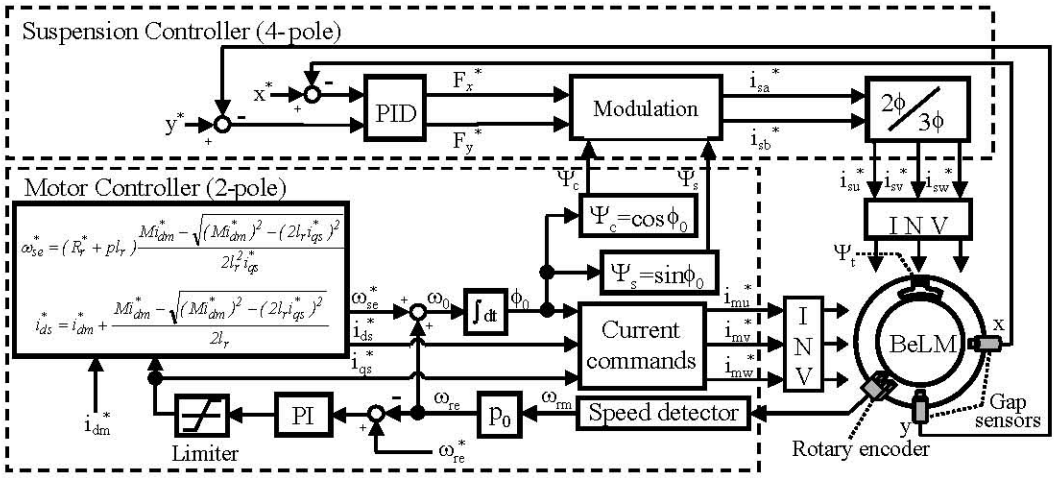

FIGURE 3: Block diagram of a bearingless motor system

force generation. If R_r^* is not exactly the same as R_r, then, the amplitude has variation and the direction has a phase-shift in the airgap flux linkage. The actual airgap flux components have phase angle error which respect to the Ψ_c and Ψ_s.

In a suspension controller, radial positions x and y are detected by displacement sensors. These displacements are compared with the reference values. The errors are amplified by Proportional–Integral–Derivative(PID) controllers to generate the suspention force commands F_x^* and F_y^*. In the modulation block, based on suspension force commands and triangular functions, suspension force winding current commands i_{sa}^* and i_{sb}^* are calculated supposing that actual airgap flux follows Ψ_c and Ψ_s. The modulation calculation is given in equation (1) as,

$$\begin{bmatrix} i_{sa}^* \\ i_{sb}^* \end{bmatrix} = \frac{M}{M'_{24}\,|\Psi_g|} \begin{bmatrix} \Psi_c & \Psi_s \\ \Psi_s & -\Psi_c \end{bmatrix} \begin{bmatrix} F_x^* \\ F_y^* \end{bmatrix} \cdots\cdots\cdots\cdots (1)$$

where

M: mutual inductance

M'_{24}: a differential value of mutual inductance between 2-pole and 4-pole windings with respect to radial displacement

$|\Psi_g|$: airgap flux amplitude ($\sqrt{\Psi_c^2 + \Psi_s^2}$)

It is seen that airgap flux errors directly cause suspension current errors, thus, actual suspension forces have discrepancies which respect to these commands F_x^* and F_y^*.

INFLUENCE VARIATION OF ROTOR RESISTANCE

Slip frequency control is sensitive to parameter variations, especially, the sensitivity of a rotor resistance is high. In practice, R_r tends to have variations because rotor temperature is dependent on operational torque and speed. In short, R_r is the minimum at starting, then, it increases as load increases. Thus, on-line real time parameter identification is basically necessary. In this section, theoretical analysis of rotor resistance variations is carried out. In addition, theoretical value is compared with empirical value. Basic idea of rotor resistance identification is provided.

In steady-state condition, ω_{se}^* and i_{ds}^* are simplified from Figure 3 as follows;

$$\omega_{se}^* = \frac{R_r^*}{2l_r^2 i_{qs}^*}\{Mi_{dm}^* - \sqrt{(Mi_{dm}^*)^2 - (2l_r i_{qs}^*)^2}\} \cdots\cdots (2)$$

$$i_{ds}^* = i_{dm}^* + \frac{Mi_{dm}^* - \sqrt{(Mi_{dm}^*)^2 - (2l_r i_{qs}^*)^2}}{2l_r} \cdots\cdots\cdots (3)$$

where,

$$l_r = L_r - M \cdots\cdots\cdots\cdots\cdots\cdots\cdots\cdots (4)$$

L_r: rotor self-inductance

The voltage and current equations of the rotor terminals in matrix form are given in equation (5), shown at the bottom of this page, where

R_s, R_r: stator and rotor resistances

L_s: stator self-inductance

ω: current angular frequency

ω_{re}: rotor shaft speed

p: differential operator (=d/dt)

subscript d, q, s and r indicates of d-axis, q-axis,

$$\begin{bmatrix} v_{ds} \\ v_{qs} \\ 0 \\ 0 \end{bmatrix} = \begin{bmatrix} R_s + pL_s & -\omega L_s & pM & -\omega M \\ \omega L_s & R_s + pL_s & \omega M & pM \\ pM & -(\omega - \omega_{re})M & R_r + pL_r & -(\omega - \omega_{re})L_r \\ (\omega - \omega_{re})M & pM & (\omega - \omega_{re})L_r & R_r + pL_r \end{bmatrix} \begin{bmatrix} i_{ds} \\ i_{qs} \\ i_{dr} \\ i_{qr} \end{bmatrix} \cdots\cdots\cdots\cdots (5)$$

stator, and rotor components, respectively.

From equation (5), the third and fourth rows can be written in steady-state condition as follows,

$$0 = -(\omega - \omega_{re})Mi_{qs} + R_r i_{dr} - (\omega - \omega_{re})L_r i_{qr} \quad \cdots\cdots(6)$$

$$0 = (\omega - \omega_{re})Mi_{ds} + (\omega - \omega_{re})L_r i_{dr} + R_r i_{qr} \quad \cdots\cdots(7)$$

The airgap fluxes Ψ_{dg} and Ψ_{qg} are defined as,

$$\Psi_{dg} = M(i_{ds} + i_{dr}) \quad \cdots\cdots(8)$$

$$\Psi_{qg} = M(i_{qs} + i_{qr}) \quad \cdots\cdots(9)$$

Solving for i_{dr} and i_{qr} in (6), (7), respectively, and subsisting into (8) and (9), the expressions for Ψ_{dg} and Ψ_{qg} are given as,

$$\Psi_{dg} = \frac{M}{R_r^2 + (\omega_{se}L_r)^2}\{(R_r^2 + \omega_{se}^2 L_r l_r)i_{ds} + \omega_{se}MR_r i_{qs}\} \quad \cdots\cdots(10)$$

$$\Psi_{qg} = \frac{M}{R_r^2 + (\omega_{se}L_r)^2}\{(R_r^2 + \omega_{se}^2 L_r l_r)i_{qs} - \omega_{se}MR_r i_{ds}\} \quad \cdots\cdots(11)$$

where ω_{se} is electrical slip frequency defined as ω-ω_{re}. Let us suppose a case when $R_r^* = R_r$. The ω_{se}^* and i_{ds}^* are given in (2) and (3), respectively. Let us substitute there command values ω_{se} and i_{ds} in (11). Let us also substitute (4), then one obtains $\Psi_{qg}=0$. This fact indicates that an airgap flux is perfectly aligned with the d-axis. In a stationary coordinate, x-axis component Ψ_{gx} of airgap flux exactly follows its reference Ψ_c. However, when $R_r^* \neq R_r$, then, $\Psi_{qg} \neq 0$. Thus, a phase difference θ_g is generated between Ψ_c and Ψ_{gx}. Substituting (2) and (3) into (10) and (11), then an expression for θ_g can be written as,

$$\theta_g = tan^{-1}\frac{\Psi_{qg}}{\Psi_{dg}} = tan^{-1}\frac{aR_r^2 + bR_r R_r^* + cR_r^{*2}}{dR_r^2 + eR_r R_r^* + fR_r^{*2}} \quad \cdots\cdots(12)$$

where coefficient a, b, c, d, e and f are defined as follows;

$$a = -2i_{qs}^{*3}l_r^4$$

$$b = -i_{qs}^* l_r M[2i_{qs}^{*2}l_r^2 + i_{dm}^* L_r\{\sqrt{(i_{dm}^* M)^2 - (2i_{qs}^* l_r)^2} - i_{dm}^* M\}]$$

$$c = i_{qs}^* l_r L_r[2i_{qs}^{*2}l_r^2 + i_{dm}^* M\{\sqrt{(i_{dm}^* M)^2 - (2i_{qs}^* l_r)^2} - i_{dm}^* M\}]$$

$$d = i_{qs}^{*2}l_r^3\{\sqrt{(i_{dm}^* M)^2 - (2i_{qs}^* l_r)^2} - i_{dm}^*(2l_r + M)\}$$

$$e = i_{qs}^{*2}l_r^2 M\{\sqrt{(i_{dm}^* M)^2 - (2i_{qs}^* l_r)^2} - i_{dm}^* M\}$$

$$f = L_r\{-i_{qs}^{*3}M^2 L_r + i_{dm}^* i_{qs}^{*2}l_r^2(2l_r + 3M) - (i_{qs}^{*2}l_r^2 - i_{dm}^{*2}ML_r)\sqrt{(i_{dm}^* M)^2 - (2i_{qs}^* l_r)^2}\}$$

Note that substituting these coefficients, $\theta_g=0$ in a case of $R_r^*=R_r$. Influence of rotor resistance variation on θ_g can be calculated from equation (12). The nominal induction motor parameters are listed in Table1.

Figure 4 shows that phase difference θ_g when R_r^*/R_r is changed between 0.5 to 2.0p.u. The calculated solid curve shows that θ_g is decreased as R_r^*/R_r is increased.

To confirm the characteristics, tooth flux waveform is monitored. The tooth flux Ψ_t is detected through an integrator connected to the terminals of search coils wound around stator teeth. It is difficult to detect airgap flux, so Ψ_t is used as reference. Then, a phase difference θ_t is obtained from the waveforms of the controller flux reference Ψ_c and the tooth flux linkage Ψ_t. The θ_t is also plotted in Figure 4. A good correspondence is seen.

TABLE 1: Parameters

Parameter		Value
Rotor self-inductance	L_r[mH]	72.46
Mutual inductance	M[mH]	68.96
Rotor leakage inductance	l_r[mH]	3.5
Rotor resistance command	R_r^*[Ω]	1.85
Magnetizing current command	i_{dm}^*[A]	2.0
Torque current command	i_{qs}^*[A]	3.5

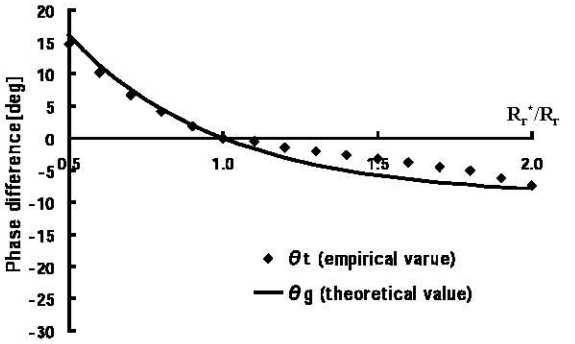

FIGURE 4: R_r^* versus phase difference

ROTOR RESISTANCE IDENTIFICATION

A. Proposed Rotor Resistance Identification System

The rotor resistance has variation depending on the torque load conditions. Thus, real time identification is necessary. The proposed rotor resistance identification system is shown in Figure 5. The rotor resistance is identified from suspension force references under static y-axis force generation to suspend a shaft weight. Basically, the shaft weight provides static force. Thus, suspension controllers generate suspension force references in opposite direction. However, when a rotor resistance rises, amplitude and direction of the suspension force references are moved so that the actual suspension force satisfies force equilibrium. Then, the rotor resistance can be estimated from the static components of the suspension force commands.

When static suspension force is aligned in y-axis, x-axis force reference indicates rotor resistance error. Thus, real time on-line identification is possible under the temperature variation.

In the figure, the Low-Pass-Filter (LPF) eliminates high frequency component to obtain dc components of the suspension force commands $F_{x\_dc}^*$. The detected $F_{x\_dc}^*$ is compared with reference value $F_{x\_dc\_ref}^*$, which is equal to zero as long as static force is aligned to the y-axis. The error is amplified in a PI controller. The estimated rotor resistance is the sum of the PI controller output and an initial value R_{r_ini}. Then, the estimated rotor resistance $\hat{R}_r$ is used in a vector controller.

B. Confirming The Operation of System

Figure 6 shows an identification process. Identification test is carried out while the reference value of the rotor resistance is set to R_r=1.48Ω (0.8p.u of genuine value). The torque current is set to i_{qs}^*=3.5A which is a half of the rated torque current value. After starting the identification process, the rotor resistance $\hat{R}_r$ is increased up to the genuine value, then, suspension force command $F_{x\_dc}^*$ is converged to zero.

Figure 7 shows the waveforms of the controller flux reference Ψ_c and the tooth flux linkage Ψ_t. Before identification process it is seen that there is a phase lead angle in the search coil flux with respect to the flux reference. The phase different is 4.63deg. After the identification, $F_{x\_dc}^*$ is converged, Ψ_c and Ψ_t are almost in phase.

Figures 8 (a) and (b) show the waveforms of the rotor radial positions x and y of the rotor shaft. Before starting the identification process, the radial positions x and y have significant fluctuations. The rotor radial fluctuation is almost 40μm(peak to peak). After, the identification is on, rotor radial displacements are better. It is seen that the rotor radial fluctuation is almost 20μm(peak to peak). Thus, the effectiveness of rotor resistance identification system is confirmed.

C. Temperature Rise Test

To confirm the effectiveness of the rotor resistance identification system, temperature rise test is carried for an hour. The torque load is about a half of the rated value so that conventional system tests can be performed stably. Two following cases are tested.

(1) The rotor resistance identification system is not used.

(2) The rotor resistance identification system is used.

In a case of (1), the rotor resistance reference R_r^* is a constant though genuine R_r is increasing as a function of time. Thus, suspension current errors are caused. The suspension forces are generated in a wrong direction. In this case, the phase difference θ_t is 4.82deg in Figure 9 at a time of 60min. The stator

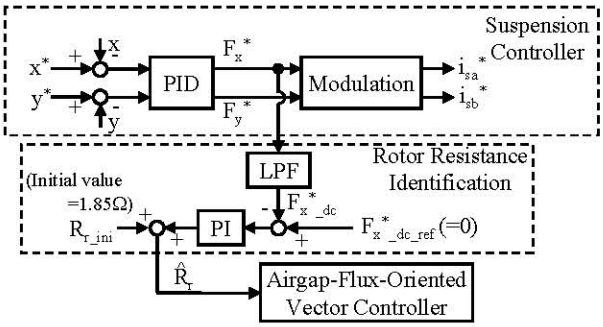

FIGURE 5: Rotor resistance identification

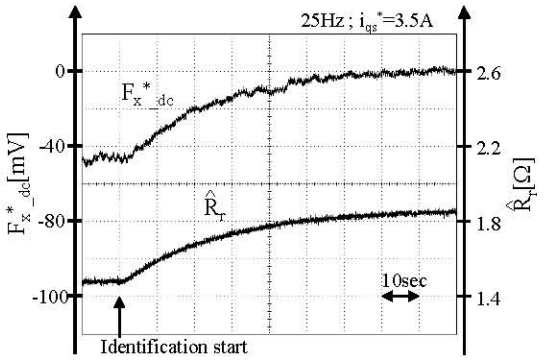

FIGURE 6: $F_{x\_dc}^*$ and $\hat{R}_r$ with rotor resistance identification

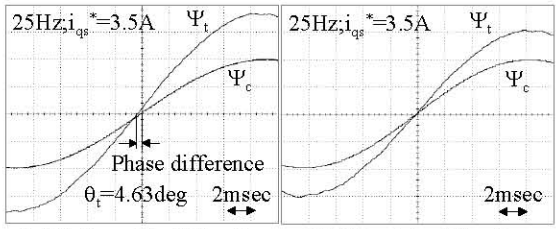

(a)Before identification (b)After identification

FIGURE 7: Phase difference between Ψ_c and Ψ_t

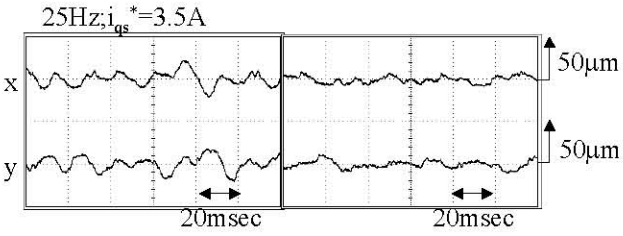

(a) Before identification (b) After identification

FIGURE 8: Waveforms of rotor radial displacements

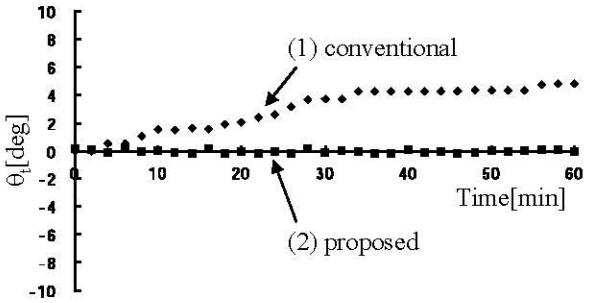

FIGURE 9: θ_t at lengthy period

temperature is 70℃. The rotor shaft has increased fluctuation.

In a case of (2), the rotor resistance R_r^* is estimated close to the actual value. Then, the phase difference is converged to zero. Thus, the shaft is successfully suspended with normal vibration level thanks to the proposed rotor resistance identification system. At the rated current, the conventional system ends up touch down although the proposed system is successful operated.

CONCLUSION

In this paper, an analysis of suspension forces considering a rotor resistance increase in an induction bearingless motor is clarified. The rotor resistance identification system based on variables in magnetic suspension loops is proposed. It is shown that the proposed rotor resistance identification system is effective in temperature rise in induction bearingless drives.

ACKNOWLEDGMENT

The authors would like to thank Mr. Shuichi Orita who was a graduate student at the Tokyo University of Science.

REFERENCE

[1] Akira Chiba, Kazuhisa Yoshida and Tadashi Fukao "Transient Response of Revolving Magnetic Field In Induction type Bearingless Motors with Secondary Resistance Variations", International Symposium on Magnetic Bearings (ISMB'98) pp.461-475 Boston, USA, Aug.7, 1998

[2] Masaru Ohsawa, Satoshi Mori and Tadashi Satoh "Study of The Induction Type Bearingless Motor", Seventh International Symposium on Magnetic Bearings, August 23-25, ISMB2000 ETH Zurich, pp.389-394

[3] Christian Redemann, Paul Meuter, Angelo Ramella, Thomas Gempp, "30KW Bearingless Canned Motor Pump on The Test Bed", ISMB pp.189-194, Aug 23-25, 2000, ETH Zurich

[4] Masahide Ooshima, Satoru Miyazawa, Akira Chiba, Fukuzo Nakamura and Tadashi Fukao, "Performance Evaluation and Test Results of a 11, 000r/min, 4kW Surface-Mounted Permanent Magnet-Type Bearingless Motor", Seventh International Symposium on Magnetic Bearings, August 23-25, ISMB2000 ETH Zurich, pp.377-382

[5] Kouhei Inagaki, Akira Chiba, M.A.Rahman and Tadashi Fukao, "Performance Characteristics of Inset-Type Permanent Magnet Bearingless Motor Drives", IEEE Power Engineering Society Winter Meeting WM2000 Conference Record CDROM Singapore 2000 January

[6] Noriaki Fujie, Rintarou Yoshimatsu, Akira Chiba, Masahide Ooshima and Tadashi Fukao, "A Decoupling Control Method of Buried Permanent Magnet Bearingless Motors Considering Magnetic Saturation", IEEJ International Power Electronics Conference IPEC 2000 Shinjuku Tokyo pp.395-400 April 3-7 2000

[7] Yutaka Kubota, Tomohiro Takenaga, Akira Chiba, "Proposed of Consequent-Pole Type Bearingless Motors" IEEJ, SPC 01-102 IEA-01-45, in Ashikaga Oct 2001(written in Japanese)

[8] Tomohiro Takenaga, Yutaka Kubota, Akira Chiba, "A Principle and A Design of A Consequent-Pole Bearingless Motor", ISMB, August 26-28, 2002, MITO, Japan. 259-264

[9] Osamu Ichikawa, Akira Chiba and Tadashi Fukao, "Principles and Structure of Homopolar Type Bearingless Motors", IEEJ International Power Electronics Conference IPEC 2000 pp.401-406 Shinjuku Tokyo pp.395-400 April 3-7 2000

[10] Akira Chiba, Masahiko Hanazawa, Tadashi Fukao and M.Azizur Rahman, "Effects of Magnetic Saturation on Radial Force of Bearingless Synchronous Reluctance Motors", IEEE Transaction on IA, vol.32, no.2, pp.354-362, 1996 March/April

[11] Masatsugu Takemoto, Ken Shimada, Akira Chiba and Tadashi Fukao, "A Design and Characteristics of Switched Reluctance Type Bearingless Motors", Fourth International Symposium on Magnetic Suspension Technology, pp.49-63, May, 1998

[12] Shuichi Orita, Takashi Nomoto, Akira Chiba, Tadashi Fukao,"Influence and Compensation of Temperature Drift in a Gap Sensor on Rotor Resistance Identification" IECEC Technical Meeting vol.102 No.43 pp.13-18 2002.05.9(written in Japanese)

[13] Takahiro Suzuki, Akira Chiba, M.Azizur Rahman and Tadashi Fukao, "An Airgap Flux Oriented Vector Controller for Stable Magnetic Suspension during High Torque Acceleration in Bearingless Induction Motors", IEEE, Industry Applications Society Annual Meeting Conference Record pp.1543-1550 Phoenix AZ Oct.3-7 1999

[14] Takahiro Suzuki, Akira Chiba, M.Azizur Rahman and Tadashi Fukao, "An Air-Gap-Flux-Oriented Vector Controller for Stable Operation of Bearingless Induction Motors", IEEE Transaction on Industry - Applications, vol.36, no.4, July/August 2000, pp.1069-1076